RSC Advances

ROYAL SOCIETY OF CHEMISTRY

www.rsc.org/advances

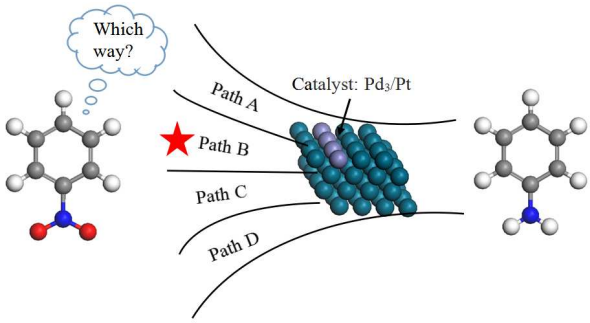

The hydrogenation mechanism of nitrobenzene to aniline on Pd_3/Pt(111) surface preferentially follows the direct route and best fit for the Jackson reaction mechanism (mechanism B).

Insights into the hydrogenation mechanism of nitrobenzene to aniline on Pd_3/Pt(111): A density functional theory study

Lianyang Zhang, Junhui Jiang, Wei Shi, Shengjie Xia, Zheming Ni*, Xuechun Xiao

College of Chemical Engineering, Zhejiang University of Technology, Hangzhou 310032, Zhejiang, China

* Corresponding author.

E–mail: jchx@zjut.edu.cn, nzm@zjut.edu.cn

Telephone number: 086–0571–88320373

Abstract:

Periodic density functional theory (DFT) calculations are performed to systematically investigate the adsorption and hydrogenation mechanism of nitrobenzene to aniline on Pd_3/Pt(111) bimetallic surface. The adsorption energies under the most stable configuration of the pertinent species are analyzed, and the activation energies and reaction energies of the possible elementary reactions are obtained. Our calculation results show that the adsorption at the Pd-top-top site through O-O atom is the most stable configuration when the nitrobenzene is perpendicular to the Pd_3/Pt(111) bimetallic surface. The hydrogenation mechanism of nitrobenzene on Pd_3/Pt(111) bimetallic surface preferentially follows the direct hydrogenation route and best fit for the Jackson reaction mechanism. Furthermore, the hydrogenation processes are almost exothermic and the hydrogenation of phenylhydroxylamine is considered as the rate-limiting step with an energetic barrier of 39.89 kcal·mol^{-1}.

Key words: Density functional theory; Nitrobenzene; Pd_3/Pt(111) bimetallic surface; Adsorption; Hydrogenation mechanism

1 Introduction

Aniline is one of the most important chemicals and intermediates in the application of pharmaceuticals, polyurethane, pesticides, explosives, pigments and dyes.[1-4] Industrial synthesis of aniline through three different routes: (i) iron powder method, (ii) selective hydrogenation of nitrobenzene (NB), (iii) electrolytic reduction

method. Till now, the selective hydrogenation of NB is likely to be the most convenient from both economical and environmental point of view,[5-7] but the common drawback was that the hydrogenation required to be performed at high pressure and/or high reaction temperature.[8,9] Therefore, the design of a catalyst, which can work under mild reaction conditions and give high catalytic performances, should be very interesting.

Recently, bimetallic nanoparticles (BMNPs) have received considerable attention for their unique catalytic properties, which are very different from the monometal due to the synergetic effects between the two metals.[10-12] Supported nanoparticles of Pt, Pd, etc., with high surface-to-volume ratio is one of the most relevant catalysts for hydrogenation of NB.[13] Liu *et al*[14] synthesized Pt-Pd/PMO-SBA-15 and the result suggested that bi-MNPs of Pt and Pd were more active than the monometallic Pt or Pd nanoparticles and the catalyst could be recovered for reuse without significant loss of catalytic activity and selectivity. Möbus *et al*[15] found that alloying with Pt leads to disaggregation down to isolated primary particles, which had a major effect on the catalytic activity (Pd 6.6, Pd/Pt 36.9 $mmol_{NB}$/min). Fan *et al*[16] compared the catalytic activities of Pt/Pd, Au/Pd and Au/Pt bimetallic nanoparticles confined in mesoporous metal oxides (MMOs=TiO_2, Al_2O_3, SiO_2, ZrO_2) in hydrogenation of NB, they found that Pd_3/Pt-m-SiO_2 showing the best catalytic activity.

Although there were extensive experimental researches on the hydrogenation reactions of NB to aniline catalyzed by Pd/Pt, the research was only focused on the activity and selectivity of this reaction, very little information exists regarding the

actual reaction mechanism. In 1898, Haber[17] first proposed a reaction path of the hydrogenation of NB based on the electrochemical reduction (Scheme 1a). It's consists in a multi-step reaction path, which comprises the step of reduction of nitro-group to nitroso-, hydroxyamino- and amino-, as well as the condensation of the intermediates to azoxybenzenes, azobenzenes, and finally to aniline. Alkaline condition favor the condensation reaction pathway. Such mechanism has been generally accepted for long time, but recently several authors raised different point of views.[18-21] In particular, Jackson and co-workers[18] proposed a new mechanism (Scheme 1b), he suggested that Pd-hydroxyamino is a common surface intermediate in the hydrogenation of nitrobenzene, whereas nitrosobenzene cannot be an intermediate if the hydrogen is sufficient. Now, there is still ongoing research in the scientific community to find out the exact reaction mechanism.

(Insert Scheme 1)

Density Functional Theory was widely used to calculate the adsorption energy, structure parameter, activation energy and reaction energy in the processes of different reactions. The current theoretical researches on the hydrogenation of NB were only focused on the mono-metallic, such as Pd,[22,23] Si,[24] Ag.[25] In this paper, we performed periodic DFT investigations on the adsorption configurations, elementary reaction processes, potential energy surfaces, and energy barrier analysis to establish the hydrogenation mechanism of NB to aniline on Pd_3/Pt(111) bimetallic surface. This

work is devoted to provide information that is complementary to that obtained from experimental studies and facilitate the determination of the complete hydrogenation reaction pathway of nitrobenzene to aniline on Pd_3/Pt catalyst. Additionally, the work provides a better understanding of the key factors that control reactivity and selectivity, which can give a guide to the rational design of Pd_3/Pt catalyst and the choice of the reaction condition.

2 Computational Details

In this work, all periodic DFT calculations were performed with the program package of DMol[3] in the Materials Studio 5.5 of Accelrys Inc,[26-28] using Perdew- Burke- Ernzerhof (PBE) generalized gradient approximation (GGA) exchange-correlation functional.[29-32] Localized double-numerical basis sets were chosen together with polarization functions (DNP). We applied Monkhorst-Pack mesh k-points of (3×3×1)[33,34] for surface calculations, and a Fermi smearing of 0.005 Hartree were used to improve the computational performance.The convergence criteria were 2×10^{-5} Ha for energy, 4×10^{-3} Ha/nm for forces, and 5×10^{-4} nm for displacement.

The Pd_3/Pt(111) surface was modeled by a periodic four-layer slab with a *p*(4×4) supercell(1/16ML), and the vacuum layer of 1.2 nm was added perpendicular to the surface, in order to avoid the interactions between periodic configurations. For all calculations, the top two layers and the adsorbed species were allowed to relax,whereas the other layers were fixed. The top and side view of Pd_3/Pt(111)

bimetallic surface models are shown in Fig. 1.

As shown in Fig.1, there are seven different adsorption sites on the Pd_3/Pt(111) surface: Pd-top, Pd-bridge, Pd-face center cubic(Pd-fcc), Pd-hexagonal close-packed (Pd-hcp), Pt-top, Pt-bridge and Pd-Pt-bridge. The adsorption energy is calculated as follows:

$$E_{ads}=E_{NB/surface}-(E_{NB}+E_{surface})$$

where $E_{NB/surface}$ is the total energy of the NB adsorption system for Pd_3/Pt(111) surface. E_a, $E_{surface}$ are the total energies of the free NB molecule and clean Pd_3/Pt(111) surface, respectively. In addition, the transition states (TSs) were derived by using the complete linear synchronous transit (LST)/quadratic synchronous transit (QST) method.[35] The convergence criteria were set to 0.01 eV and all TSs were confirmed by the vibrational frequency analysis.

(Insert Figure 1)

3 Result and discussion

In order to clarify the reaction of NB hydrogenation to aniline on the Pd_3/Pt(111) surface, we first describe the most stable configurations of NB, then we discuss all possible elementary reaction steps in detail.

3.1 Adsorption process

According to the structure of NB molecule and research results of other investigators, there are two possible adsorption models:[36,37] Parallel adsorption and

vertical adsorption. We consider 21 different adsorption sites on Pd_3/Pt(111) surface for each adsorption mode, which included N, O monatomic adsorption and O-O, N-O biatomic adsorption. The adsorption energies of NB are summarized in Table 1.

(Insert Table 1)

After optimization, we compared 42 different adsorption configurations, the results show that the model of vertical adsorption is superior to the parallel adsorption, this is in good agreement with references.[38,39] The initial site of Pd-top-top through O-O found to be the most stable configuration with the adsorption energy of -22.37 kcal·mol^{-1}, meanwhile, the N atom was adsorbed on bridge site. The distance between the Pd atom and O atom is 0.2348 nm and 0.2325 nm, respectively, and the angle of O-N-O is 123.45º. The optimized structure of isolated NB and the schematic diagram of the most stable configurations of NB on Pd_3/Pt(111) surface is shown in Fig. 2.

(Insert Figure 2)

In order to highlight the adsorption of NB molecule on Pd_3/Pt(111) surface, we calculated the partial density of states (PDOS) for the *p*-orbitals of NB molecules before and after adsorption, as shown in Fig. 3. The Fermi level is set to zero. The PDOS below the Fermi level represent the highest occupied molecular orbital (HOMO), while between the 0-15 eV represent the lowest unoccupied molecular

orbital (LUMO).

(Insert Figure 3)

From the curve for PDOS of NB molecule, it can be seen that the peak at -2.5 eV is attributed to the lone pair electrons of O atom and the peak at -8.0 eV is attributed to the lone pair electrons of N atom. When NB adsorbed on M(111) surface, the PDOS peaks before Fermi level decreased and shifted to lower energy. In addition, the peaks of LUMO disappeared. This indicated that there was a strong interaction between π bond of NB and the *d*-orbitals of Pd_3/Pt(111) surface.

3.2 Reaction pathways

On the basis of previous research results[17,18], we studied four possible hydrogenation mechanism of NB to aniline on Pd_3/Pt(111) surface systematically. Table 2 provides four possible hydrogenation mechanisms of NB on a Pd_3/Pt(111) surface. As shown in Table 2, the mechanism A, B represent the direct route and C, D represent the condensation route. We optimized the structures of the reactants (IS) and products (FS) for each elementary reaction, and then searched the transition state (TS). The activation energies and reaction energies of the TSs are listed in Table 3.

(Insert Table 2)

(Insert Table 3)

3.2.1 Direct reaction pathways(mechanism A and mechanism B)

Comparing the mechanism A and mechanism B, the main difference between the two mechanisms is the formation of C_6H_5NOH, including step(2) and step(3), so we only compare this two steps of hydrogenation processes. The activation energies and reaction energies of IS, TS and FS in the mechanisms of step(2) and step(3) are presented in Fig. 4.

(Insert Figure 4)

$C_6H_5NO_2H^*+H^*\rightarrow C_6H_5NO^*+H_2O^*$. The optimal co-adsorption configurations of $C_6H_5NO_2H$+H and C_6H_5NO+H_2O were defined as IS1 and FS1, respectively, which were both calculated. The $C_6H_5NO_2H$ rotated clockwise and inclined to the top site through the O atom, the atomic H was adsorbed on the fcc site. In TS1, the N-O bond was broken and the O-H was formed. The distance between the atomic H and the cracked O atom was decreased from 0.2980 to 0.2041 nm. For FS1, the C_6H_5NO was turned to right and tilted downward to the hollow site through the O atom, the H_2O was adsorbed on the top site through O atom. This reaction was exothermic by 33.67 kcal·mol^{-1}, and the corresponding E_a was 44.28 kcal·mol^{-1}.

$C_6H_5NO^*+H^*\rightarrow C_6H_5NOH^*$, the structure of C_6H_5NO and the atomic H remained the same as the initial state. In TS2, the atomic H left the fcc site and moved to the adjacent top site to get close to the C_6H_5NO, the distance of the reacted O-H was 0.1730 nm. For FS2, the C_6H_5NOH adsorbed at the top site via the O atom, the

bond length of the reacted O-H was 0.0999 nm. This reaction was exothermic by 1.38 kcal·mol^{-1}, and the corresponding E_a was 24.44 kcal·mol^{-1}.

$C_6H_5NO_2H^*+H^*\rightarrow C_6H_5NO_2H_2^*$, the reactant was the same as what was described in IS1. In TS3, the atomic H left fcc site and moved far away from the Pd_3/Pt(111) surface, the $C_6H_5NO_2H$ sloped downward to meet the attacking H atom. The distance of of the reacted O-H decreased from 0.2569 nm to 0.1498 nm. Once FS3 was formed, the $C_6H_5NO_2H_2$ further sloped downward and the H moved upward. The bond length of the reacted O-H was 0.0987 nm. This reaction was exothermic by 5.30 kcal·mol^{-1}, and the corresponding E_a was 26.98 kcal·mol^{-1}.

$C_6H_5NO_2H_2^*+H^*\rightarrow C_6H_5NOH^*+H_2O^*$, we calculated the co-adsorption of $C_6H_5NO_2H_2$ and atomic H as IS4. After adsorption, the atomic H located at the fcc site, the $C_6H_5NO_2H_2$ rotated anticlockwise, and finally adsorbed at the bridge-top site through the bond of N-O. In TS4, the atomic H moved close to the reacted O-H, resulting in a shortening of the distance between the O-H and atomic H (from 0.3453 nm to 0.2250 nm). Moreover, one of the N-O bonds broke up. For FS2, the C_6H_5NOH adsorbed at bridge-bridge site through the bond of N-O, and the H_2O tilted adsorbed on the top site through the O atom. This reaction was exothermic by 31.13 kcal·mol^{-1}, and the corresponding E_a was 28.83 kcal·mol^{-1}.

Based on the activation energies and the reaction energies, the one-dimensional potential energy surface diagram of mechanism A and B were summarized in Fig. 5. We can see that no matter what kind of processes they were, the reaction was exothermic. By comparing the activation energy with different processes, the

activation energy of mechanism A was higher than B, this indicated that the mechanism B was significantly easier to occur than mechanism A does. Moreover, in mechanism B, the hydrogenation of phenylhydroxylamine has the highest activation barrier and could be the rate-limiting step because of the cleavage of the N-O bond.

(Insert Figure 5)

3.2.2 Condensation reaction pathways(mechanism C and mechanism D)

The main differences between mechanism C and D are step(2), step(3) and step(4). The step(2) and step(3) had been discussed in direct reaction pathways, so we only compared the step of the forming of azoxybenzene. The activation energies and reaction energies of IS, TS and FS in the mechanisms of step(2) and step(3) were presented in Fig. 6.

(Insert Figure 6)

$C_6H_5NO^*+C_6H_5NHOH^*\rightarrow C_{12}H_{10}N_2O^*+H_2O^*$, We calculated the advantages of co-adsorption configuration of $C_6H_5NO^*$ and $C_6H_5NHOH^*$ as IS5. The C_6H_5NO adsorbed at the top site through O atom and the C_6H_5NHOH adsorbed at the bridge site through O atom. In TS5, the reacted H_2O moved downward away from the $C_{12}H_{10}N_2O$ and close to the Pd_3/Pt(111) surface. In FS5, the benzene ring which close to the N-O bond was rotated anticlockwise and the other benzene ring maintain the

same, the H_2O inclined to adsorbed on the top site through the O atom. This reaction was exothermic by 43.12 kcal·mol^{-1}, and the corresponding E_a was 52.12 kcal·mol^{-1}.

$2C_6H_5NOH^* \rightarrow C_{12}H_{10}N_2O^* + H_2O^*$, this reaction began with the co-adsorption of two C_6H_5NOH molecule (IS6), after adsorption, the top of two C_6H_5NOH molecules moved closer together, and the space between tapers, but the space between the bottom of the molecules became larger. In TS6, the forming H_2O adsorbed on the hollow site through the O atom and the length of O-H in H_2O molecule decreased from 0.3531 nm to 0.2754 nm, the length of N=N bond decreased from 0.1370 nm to 0.1288 nm. The product is the same as FS5. This reaction was exothermic by 50.96 kcal·mol^{-1}, and the corresponding E_a was 90.63 kcal·mol^{-1}.

Based on the activation energies and the reaction energies, the one-dimensional potential energy surface diagram of mechanism C and D are summarized in Fig. 7. The condensation reaction is complex and had many steps, so we only draw the different steps in Fig. 7. The results indicated that the overall condensation reaction pathways are highly exothermic, the energetic difference between the two pathways are obvious. The mechanism C has one more step than mechanism D, but the activation barrier is lower than D, especially the formation of azoxybenzene, which is the rate-limiting step.

(Insert Figure 7)

3.3 Brief summary about NB hydrogenation

We have investigated the overall reactions involving the direct reaction and condensation reaction pathways of NB hydrogenation. By comparing the mechanism of the different hydrogenation process, we can find that all these processes are exothermic, and the energy barrier of mechanism B is the lowest, the low barrier along with the endothermicity makes mechanism B a likely path on Pd_3/Pt(111), similar to that suggested by Jackson and co-workers. The formation of C_6H_5NH* from phenylhydroxylamine is considered as the rate-limiting step, which has the highest energy barrier because of the cleavage of the N-O bond.

4 Conclusion

In this work, the adsorption and the hydrogenation mechanism of NB to aniline on Pd_3/Pt(111) surface have been systematically investigated by using DFT calculations at the molecular level. We identify the optimal adsorption model and preferred reaction path of NB hydrogenation.

Our results show that there is a strong interaction between π bond of NB and the *d*-orbitals of Pd_3/Pt(111) surface, the vertical adsorption of NB at the Pd-top-top site through O-O atom is the most adsorption configuration.

No matter what kind of mechanism it follows, the NB hydrogenation process is almost exothermic. The phenylhydroxylamine is proposed to be the key intermediate product for the hydrogenation of NB. Mechanism B is the most likely path on Pd_3/Pt(111), and the formation of C_6H_5NH* from phenylhydroxylamine is considered as the rate-limiting step. Thus, it can be concluded that lower pH value of solution

was beneficial to the hydrogenation of NB.

References

1 W. J. Sandborn, *Am J. Gastroenterol*. 2002, **97**, 2939-2941.

2 R. S. Downing, P. J. Kunkeler and H. van Bekkum, *Catal. Today*, 1997, **37**, 121-136.

3 X. Meng, H. Cheng, Y. Akiyama, Y. Hao, W. Qiao, Y. Yu, F. Zhao, S. I. Fujita and M. Arai, *J. Catal.*, 2009, **264**, 1-10.

4 E. Merino, *Chem. Soc. Rev.* 2011, **40**, 3835-3853.

5 S. K. Tanielyan, J. J. Nair, N. Marin, G. Alvez, R. J. McNair, D. Wang and R. L. Augustine, *Org. Proc. Res. Dev.,* 2007, **11**, 681-688.

6 K. Min, J. Choi, Y. Chung, W. Ahn, R. Ryoo and P. K. Lim, *Appl. Catal. A: Gen.,* 2008, **337**, 97-104.

7 C.V. Rode, M.J. Vaidya, R. Jaganathan and R.V. Chaudhari, *Chem. Eng. Sci.,* 2001, **56**, 1299-1304.

8 F. Y. Zhao, Y. Ikushima and M. Arai, *J. Catal.,* 2004, **224**, 479-483.

9 J. M. Nadgeri, M. M. Telkar and C. V. Rode, *Catal. Commun.*, 2008, **9**, 441-446.

10 T. Wu, D. J. Childers, C. Gomez, A. M. Karim, N. M. Schweitzer, A. J. Kropf, H. Wang, T. B. Bolin, Y. Hu, L. Kovarik, R. J. Meyer and J. T. Miller, *ACS Catal.*, 2012, **2**, 2433-2443.

11 R. T. Mu, Q. A. Fu, H. Xu, H. I. Zhang, Y. Y. Huang, Z. Jiang, S. O. Zhang, D. L.

Tan and X. H. Bao, *J. Am. Chem. Soc.*, 2011, **133**, 1978-1986.

12 S. I. Sanchez, M. W. Small, J. M. Zuo and R. G. Nuzzo, *J. Am. Chem. Soc.*, 2009, **131**, 8683-8689.

13 P. Maity, S. Basu, S. Bhaduri and G. K. Lahiri, *Adv. Synth. Catal.* 2007, **349**, 1955-1962.

14 C. Liu, R. Tan, N. Y. Yu and D. H. Yin, *Microporous and Mesoporous Materials*, 2010, **131**, 162-169.

15 K. Möbus, E. Grünewald, S. D. Wieland, S. F. Parker and P .W. Albers, *J. Catal.*, 2014, **313**, 153-160.

16 J. J. Liu, S. H. Zou, L. P. Xiao and J. Fan, *Catal. Sci. Technol.*, 2014, **4**, 441-446.

17 F. Haber, *Z. Elektrochem.* 1898, **22**, 506–512.

18 E. A. Gelder, S. D. Jackson and C. M. Lok, *Chem. Commun.*, 2005, 522-524.

19 A. Corma and P. Serna, *Science*, 2006, **313**, 332-334.

20 H. U. Blaser, *Science*, 2006, **313**, 312-313.

21 A. Corma, P. Concepcion and P. Serna, *Angew. Chem. Int. Ed*. 2007, **46**, 7266-7269.

22 J. H. Lyu, J. G. Wang, C. S. Lu, L. Ma, Q. F. Zhang, X. B. He, and X. N. Li, *J. Phys. Chem. C*, 2014, **118**, 2594−2601.

23 M. Chatterjee, A. Chatterjee, H. Kawanami, T. Ishizaka, T. Suzuki and A. Suzuki, *Adv. Synth. Catal.* 2012, **354**, 2009-2018.

24 F. Y. Tian, Y. X. Cui and A. V. Teplyakov, *J. Phys. Chem. C.* 2014, **118**, 502-512.

25 L. B. Zhao, Y. F. Huang, X. M. Liu, J. R. Anema, D. Y. Wu, B. Ren and Z. Q.

Tian, *Phys. Chem. Chem. Phys.*, 2012, **14**, 12919-12929.

26 B. Delley, *J. Chem. Phys.* 1990, **92**, 508-517.

27 B. Delley, *J. Chem. Phys.* 2000, **113**, 7756-7764.

28 W. Shi, L. Y. Zhang, Z. M. Ni, X. C. Xiao and S. J. Xia, *RSC Adv.*, 2014, **4**, 27003-27012.

29 Z. G. Deng, X. Q. Lu, Z. Q. Wen, S. X. Wei, Q. Zhu, D. L. Jin, X. F. Shi and W. Y. Guo, *RSC Adv.*, 2014, **4**, 12266-12274.

30 J. P. Perdew, K. Burke and M. Ernzerhof, *Rev. Lett.* 1996, **77**, 3865-3868.

31 L. Y. Zhang, W. Shi, S. J. Xia and Z. M. Ni, *Acta Phys. -Chim. Sin.*, 2014, **30**, 1847-1854.

32 S. C. Yeo, S. S. Han and H. M. Lee. *J. Phys. Chem. C,* 2014, **118**, 5309-5316.

33 Q. Meng, Y. Shen, J. Xu and J. Gong, *Chin. J. Catal.*, 2012, **33**, 407-415

34 H. J. Monkhorst and J. D. Pack, *Phys. Rev: B,* 1976, **13**, 5188-5192.

35 T. A. Halgren and W. N. Lipscomb, *Chem. Phys. Lett.*, 1977, **49**, 225-232.

36 J. H. Lyu, J. G. Wang, C. H. Lu, L. Ma, Q. F. Zhang, X. B. He and X. N. Li, *J. Phys. Chem. C*, 2014, **118**, 2594−2601.

37 F. Y. Tian, Y. X. Cui and A. V. Teplyakov, *J. Phys. Chem. C*, 2014, **118**, 502-512.

38 J. J. Mortensen, M. V. Ganduglia-Pirovano, L. B. Hansen, B. Hammer, P. Stoltze and J. K. Norskov, *Surf. Sci.*, 1999, **422**, 8-16.

39 S. Q. Zhou, D. H. Li, F. Q. Zhao and X. H. Ju, *Struct Chem.*, 2014, **25**, 409-417.

Figure Captions

Scheme 1. The different hydrogenation mechanism of NB to aniline

Pd_{surf}: metallic surface of the Pd catalyst.

(a) Haber reaction mechanism; (b) Jackson reaction mechanism

Fig. 1 Structural configuration of 4×4 supercell containing four layers of Pd_3/Pt(111) bimetallic surface

Fig. 2 The structure of NB and its most stable configuration on Pd_3/Pt(111) bimetallic surface

(a) Nitrobenzene molecule; (b) The top view; (c) The side view

Fig. 3 *p* orbitals projected density of states(PDOS) of NB molecule before and after adsorption

Fig. 4 The IS, TS, and FS of elementary reactions in A(2), A(3), B(2) and B(3) on Pd_3/Pt(111) bimetallic surface. The A and B are reaction mechanisms as in Table 2.

Fig. 5 The one-dimensional potential energy surface diagram of mechanism A and B. The parts of the energy barrier shown in bold represent the rate limiting steps of the corresponding mechanism.

Fig. 6 The IS, TS, and FS of elementary reactions in C(5) and D(6) on Pd_3/Pt(111) plane. The C and D are reaction mechanisms as in Table 2.

Fig. 7 The one-dimensional potential energy surface diagram of mechanism C and D. The parts of the energy barrier shown in bold represent the rate limiting steps of the corresponding mechanism.

Table Captions

Table 1 Adsorption energy (E_{ads}) of NB molecule on Pd_3/Pt(111) bimetallic surface

Table 2 Reaction mechanisms of A-D for the hydrogenation of NB on Pd_3/Pt(111) bimetallic surface

Table 3 Calculated activation energies (Ea) and reaction energies (ΔE) of main elementary reactions on Pd_3/Pt(111) bimetallic surface

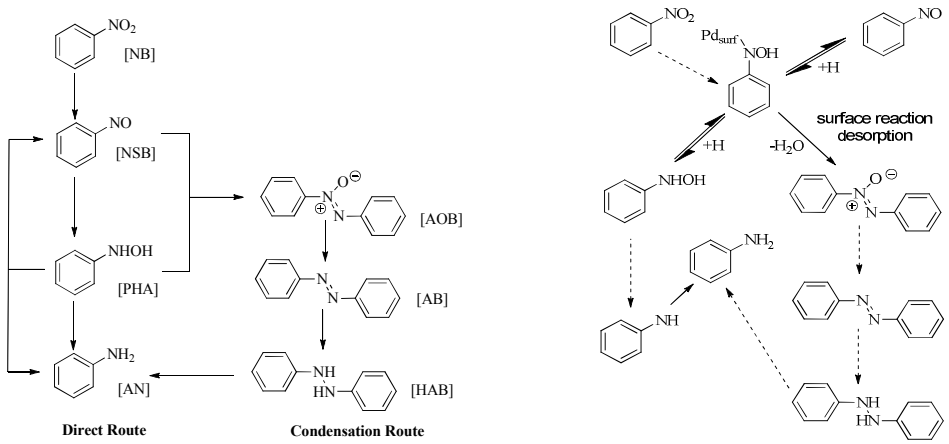

(a) (b)

Scheme 1. The different hydrogenation mechanism of NB to aniline

Pd_{surf}: metallic surface of the Pd catalyst.

(a) Haber reaction mechanism (b) Jackson reaction mechanism

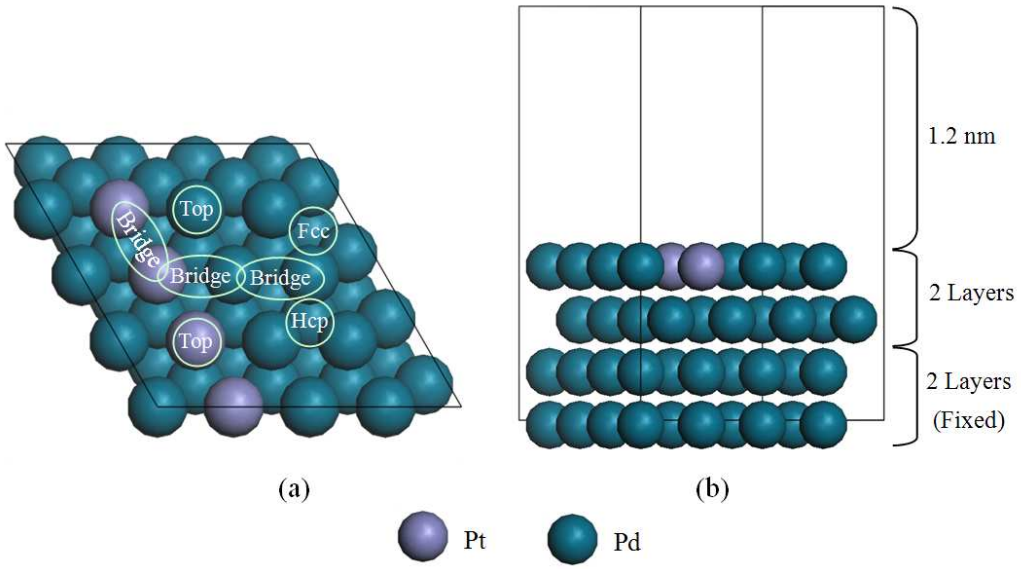

Fig. 1 Structural configuration of 4×4 supercell containing four layers of Pd_3/Pt(111) bimetallic surface

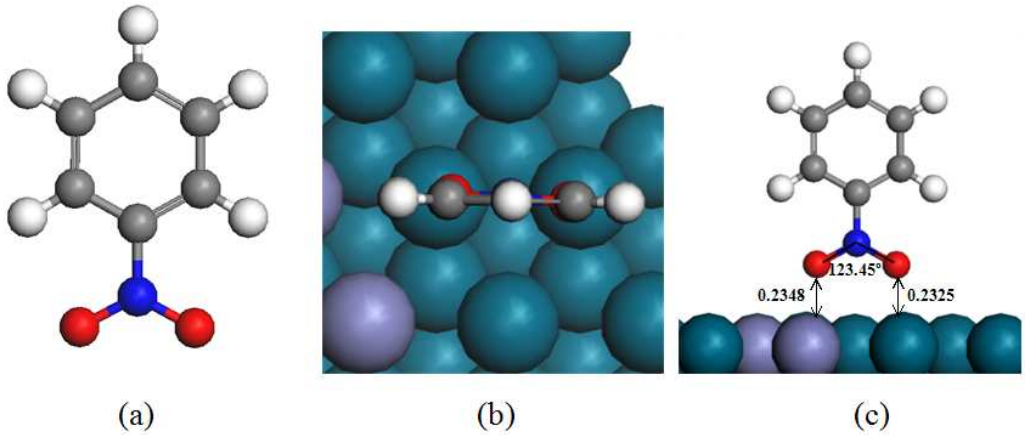

Fig. 2 The structure of NB and its most stable configuration on Pd_3/Pt(111) bimetallic surface

(a) Nitrobenzene molecule; (b) The top view; (c) The side view

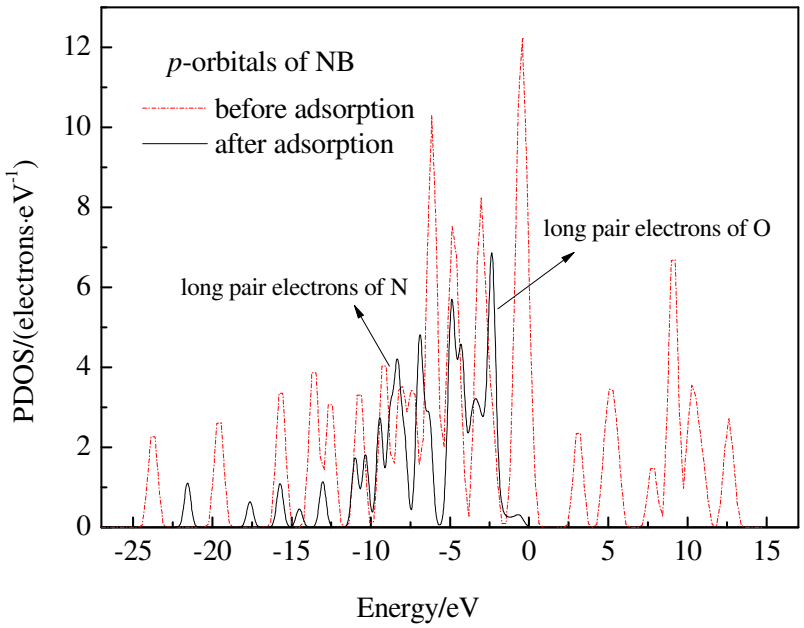

Fig. 3 *p* orbitals projected density of states(PDOS) of NB molecule before and after adsorption

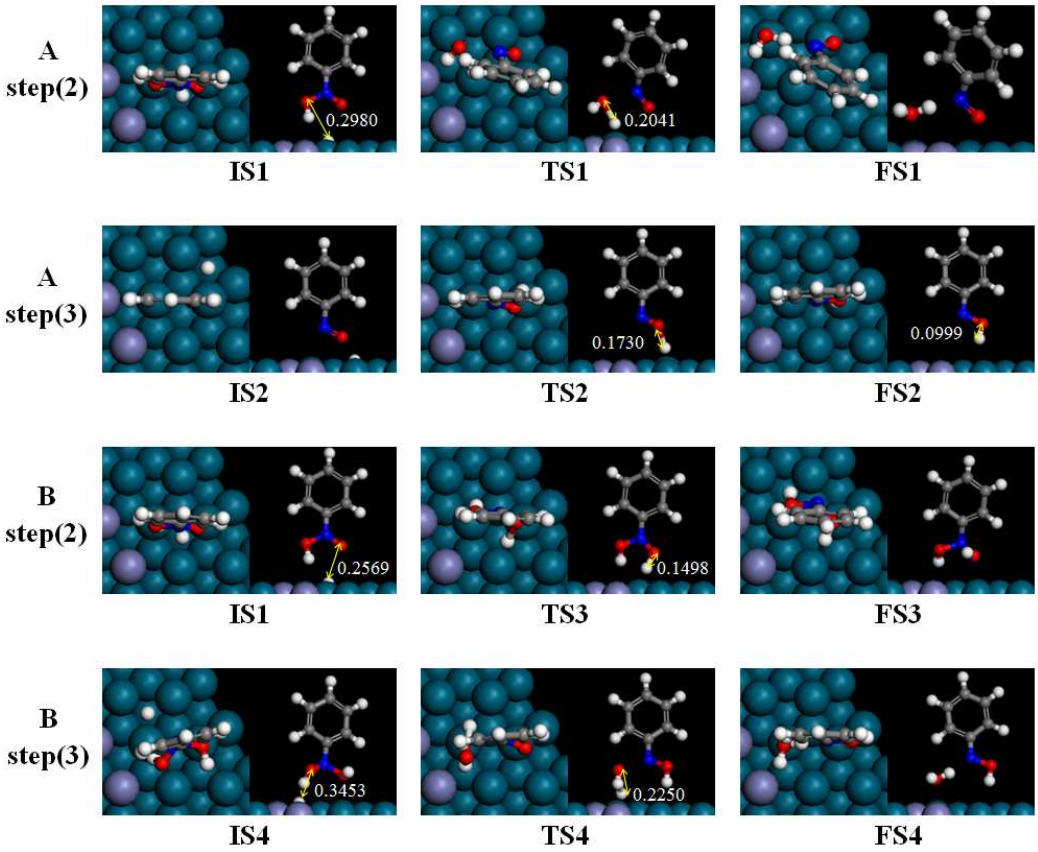

Fig. 4 The IS, TS, and FS of elementary reactions in A(2), A(3), B(2) and B(3) on Pd_3/Pt(111) bimetallic surface. The A and B are reaction mechanisms as in Table 2.

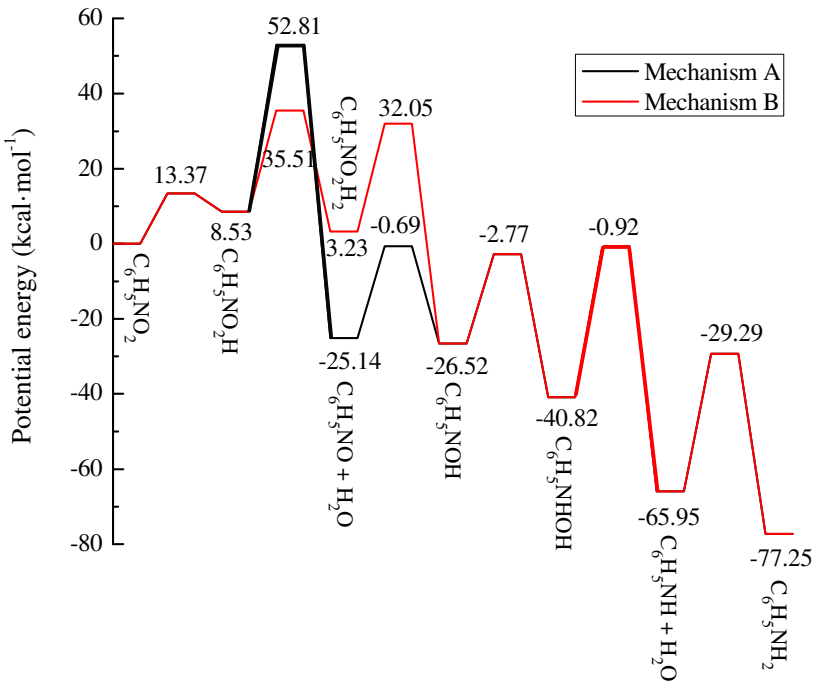

Fig. 5 The one-dimensional potential energy surface diagram of mechanism A and B. The parts of the energy barrier shown in bold represent the rate limiting steps of the corresponding mechanism.

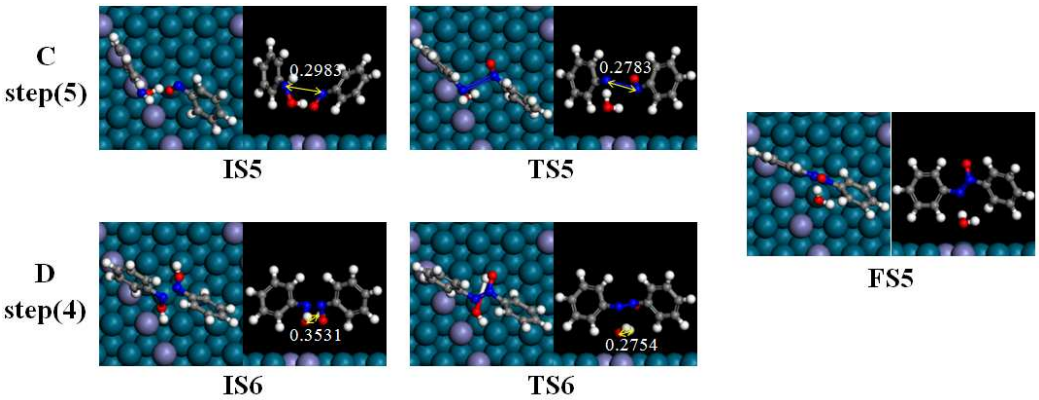

Fig. 6 The IS, TS, and FS of elementary reactions in C(5) and D(6) on Pd_3/Pt(111) plane. The C and D are reaction mechanisms as in Table 2.

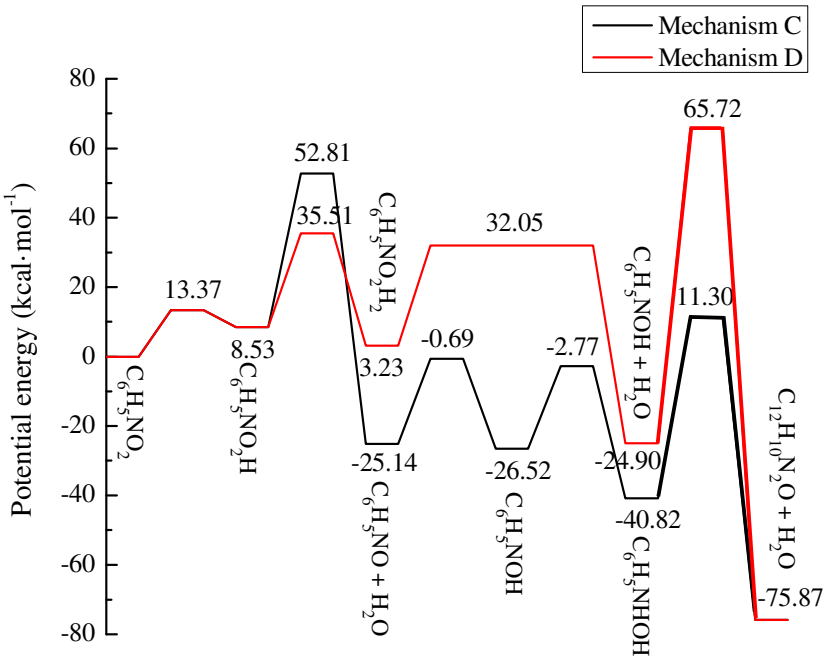

Fig. 7 The one-dimensional potential energy surface diagram of mechanism C and D. The parts of the energy barrier shown in bold represent the rate limiting steps of the corresponding mechanism.

Table 1 Adsorption energy (E_{ads}) of NB molecule on Pd_3/Pt(111) bimetallic surface

	Initial adsorption position	**E_{ads} /(kcal·mol^{-1})**	**Initial adsorption position**	**E_{ads} /(kcal·mol^{-1})**
	Pd-top-N	-16.37	Pt-top-O-O	-17.30
	Pd-top-O	-18.68	Pd-bridge-N	-19.60
	Pd-top-O-O	-20.06	Pd-bridge-O	-20.06
	Pd-hcp-N	-19.83	Pd-bridge-O-O	-18.91
	Pd-hcp-O	-19.60	Pt-bridge-N	-17.30
parallel	Pd-hcp-O-O	-16.14	Pt-bridge-O	-17.06
	Pd-fcc-N	-18.68	Pt-bridge-O-O	-17.76
	Pd-fcc-O	-19.37	Pd-Pt-bridge-N	-17.53
	Pd-fcc-O-O	-20.29	Pd-Pt-bridge-O	-17.30
	Pt-top-N	-16.14	Pd-Pt-bridge-O-O	-16.83
	Pt-top-O	-17.53		
	Pd-top-N	-20.06	Pt-top-O-O	-16.83
	Pd-top-O	-21.45	Pd-bridge-N	-21.45
	Pd-top-O-O	-22.37	Pd-bridge-O	-21.22
	Pd-hcp-N	-21.22	Pd-bridge-O-O	-21.22
	Pd-hcp-O	-20.75	Pt-bridge-N	-16.37
vertical	Pd-hcp-O-O	-17.06	Pt-bridge-O	-16.83
	Pd-fcc-N	-21.45	Pt-bridge-O-O	-14.53
	Pd-fcc-O	-21.22	Pd-Pt-bridge-N	-18.45
	Pd-fcc-O-O	-16.14	Pd-Pt-bridge-O	-18.68
	Pt-top-N	-14.99	Pd-Pt-bridge-O-O	-20.06
	Pt-top-O	-16.37		

Table 2 Reaction mechanisms of A-D for the hydrogenation of NB on Pd_3/Pt(111) bimetallic surface

Steps	Mechanism A	Mechanism B
(1)	$C_6H_5NO_2$*+H*→$C_6H_5NO_2H$*	$C_6H_5NO_2$*+H*→$C_6H_5NO_2H$*
(2)	$C_6H_5NO_2H$*+H*→C_6H_5NO*+H_2O*	$C_6H_5NO_2H$*+H*→$C_6H_5NO_2H_2$*
(3)	C_6H_5NO*+H*→C_6H_5NOH*	$C_6H_5NO_2H_2$*+H*→C_6H_5NOH*+H_2O*
(4)	C_6H_5NOH*+H*→C_6H_5NHOH*	C_6H_5NOH*+H*→C_6H_5NHOH*
(5)	C_6H_5NHOH*+H*→C_6H_5NH*+H_2O*	C_6H_5NHOH*+H*→C_6H_5NH*+H_2O*
(6)	C_6H_5NH*+H*→$C_6H_5NH_2$*	C_6H_5NH*+H*→$C_6H_5NH_2$*
	Mechanism C	**Mechanism D**
(1)	$C_6H_5NO_2$*+H*→$C_6H_5NO_2H$*	$C_6H_5NO_2$*+H*→$C_6H_5NO_2H$*
(2)	$C_6H_5NO_2H$*+H*→C_6H_5NO*+H_2O*	$C_6H_5NO_2H$*+H*→$C_6H_5NO_2H_2$*
(3)	C_6H_5NO*+H*→C_6H_5NOH*	$C_6H_5NO_2H_2$*+H*→C_6H_5NOH*+H_2O*
(4)	C_6H_5NOH*+H*→C_6H_5NHOH*	
(5)	C_6H_5NO*+C_6H_5NHOH*→$C_{12}H_{10}N_2O$*+H_2O*	2C_6H_5NOH*→$C_{12}H_{10}N_2O$*+H_2O*
(6)	$C_{12}H_{10}N_2O$*+H*→$C_{12}H_{10}N_2OH$*	$C_{12}H_{10}N_2O$*+H*→$C_{12}H_{10}N_2OH$*
(7)	$C_{12}H_{10}N_2OH$*+H*→$C_{12}H_{10}N_2$*+H_2O*	$C_{12}H_{10}N_2OH$*+H*→$C_{12}H_{10}N_2$*+H_2O*
(8)	$C_{12}H_{10}N_2$*+H*→$C_{12}H_{10}N_2H$*	$C_{12}H_{10}N_2$*+H*→$C_{12}H_{10}N_2H$*
(9)	$C_{12}H_{10}N_2H$*+H*→$C_{12}H_{10}N_2H_2$*	$C_{12}H_{10}N_2H$*+H*→$C_{12}H_{10}N_2H_2$*
(10)	$C_{12}H_{10}N_2H_2$*+H*→$C_6H_5NH_2$*+C_6H_5NH*	$C_{12}H_{10}N_2H_2$*+H*→$C_6H_5NH_2$*+C_6H_5NH*
(11)	$C_6H_5NH_2$*+C_6H_5NH*+H*→2$C_6H_5NH_2$*	$C_6H_5NH_2$*+C_6H_5NH*+H*→2$C_6H_5NH_2$*

Table 3 Calculated activation energies (*E*a) and reaction energies (Δ*E*) of main elementary reactions on Pd_3/Pt(111) bimetallic surface

Reactions	E_a /(kcal·mol^{-1})	Δ*E* /(kcal·mol^{-1})
$C_6H_5NO_2$*+H*→$C_6H_5NO_2H$*	13.37	8.53
$C_6H_5NO_2H$*+H*→C_6H_5NO*+H_2O*	44.28	-33.67
$C_6H_5NO_2H$*+H*→$C_6H_5NO_2H_2$*	26.98	-5.30
C_6H_5NO*+H*→C_6H_5NOH*	24.44	-1.38
$C_6H_5NO_2H_2$*+H*→C_6H_5NOH*+H_2O*	28.83	-31.13
C_6H_5NOH*+H*→C_6H_5NHOH*	23.75	-14.30
C_6H_5NHOH*+H*→C_6H_5NH*+H_2O*	39.89	-25.14
C_6H_5NH*+H*→$C_6H_5NH_2$*	36.67	-11.30
C_6H_5NO*+C_6H_5NHOH*→$C_{12}H_{10}N_2O$*+H_2O*	52.12	-43.12
2C_6H_5NOH*→$C_{12}H_{10}N_2O$*+H_2O*	90.63	-50.96
$C_{12}H_{10}N_2O$*+H*→$C_{12}H_{10}N_2OH$*	62.49	11.30
$C_{12}H_{10}N_2OH$*+H*→$C_{12}H_{10}N_2$*+H_2O*	28.13	-46.58
$C_{12}H_{10}N_2$*+H*→$C_{12}H_{10}N_2H$*	74.95	-6.00
$C_{12}H_{10}N_2H$*+H*→$C_{12}H_{10}N_2H_2$*	23.75	-17.53
$C_{12}H_{10}N_2H_2$*+H*→$C_6H_5NH_2$*+C_6H_5NH*	60.65	-20.06
$C_6H_5NH_2$*+C_6H_5NH*+H*→2$C_6H_5NH_2$*	41.97	28.36